A critical comparison of equilibrium, non-equilibrium and boundary-driven molecular dynamics techniques for studying transport in microporous materials

Gaurav Arya, Hsueh-Chia Chang, and Edward J. Maginn[a)]
Department of Chemical Engineering, University of Notre Dame, Notre Dame, Indiana 46556

(Received 26 April 2001; accepted 8 August 2001)

Transport in an idealized model with variable pore diameter as well as an $AlPO_4$-5 zeolite is examined using three different molecular dynamics techniques: (1) equilibrium molecular dynamics (EMD); (2) external field nonequilibrium molecular dynamics (EF–NEMD); and (3) dual control volume grand canonical molecular dynamics (DCV–GCMD). The EMD and EF–NEMD methods yield identical transport coefficients for all the systems studied. The transport coefficients calculated using the DCV–GCMD method, however, tend to be lower than those obtained from the EMD and EF–NEMD methods unless a large ratio of stochastic to dynamic moves is used for each control volume, and a streaming velocity is added to all inserted molecules. Through development and application of a combined reaction–diffusion–convection model, this discrepancy is shown to be due to spurious mass and momentum transfers caused by the control volume equilibration procedure. This shortcoming can be remedied with a proper choice of streaming velocity in conjunction with a well-maintained external field, but the associated overhead makes it much less efficient than either the EMD or EF–NEMD techniques. © *2001 American Institute of Physics.* [DOI: 10.1063/1.1407002]

I. INTRODUCTION

The transport of guest species confined within microporous hosts has important ramifications in areas such as membranes, catalysis, and adsorption. When the size of the diffusing species becomes commensurate with the size of the confining pores, peculiar phenomena not seen in bulk systems are observed.[1] There has been a great deal of effort recently to better understand the phenomena associated with transport in these materials, including experimental[2] and theoretical,[3,4] approaches. Molecular simulations also have become a valuable tool in examining these systems. Three comprehensive reviews of simulation methods used to examine diffusion in these systems have appeared recently.[5–7]

The quantity most often of interest in studies of transport of these guest species under concentration gradients is the *transport diffusivity*, D_t. The above nonequilibrium mode of transport is generally described by the Fickian constitutive relation

$$\mathbf{J} = -D_t(c)\nabla c, \tag{1}$$

where $\mathbf{J}$ is the molecular diffusive flux and ∇c is the spatial concentration gradient, presumed to drive diffusion. An alternative formulation which relates the molecular diffusive flux to a driving force is based on the Onsager and Maxwell–Stefan (MS) formulations of irreversible thermodynamics.[8] This formulation presupposes that the driving force for isothermal diffusive mass transport is a gradient in chemical potential rather than a concentration gradient. Thus the MS constitutive relation for a single component diffusing in a stationary host is

$$\mathbf{J} = -\frac{L(c)}{k_B T}\nabla \mu, \tag{2}$$

where $L(c)$ is the single component transport coefficient, k_B is the Boltzmann constant, T is temperature and μ is the chemical potential. Equation (2) can readily be extended to treat mixtures.[9] The usefulness and validity of the MS approach for modeling transport in microporous materials has been confirmed by several authors.[10,11] The primary focus of this paper will be on computing the MS transport coefficient L, since the two nonequilibrium transport coefficients can be related to one another through knowledge of the adsorption isotherm via the following relation:[12]

$$D_t(c) = \frac{L(c)}{k_B T}\frac{\partial \mu}{\partial c}. \tag{3}$$

There are four general classes of methods that have been used to compute the MS transport coefficient L. The methods are summarized below.

A. Equilibrium molecular dynamics

Given certain reasonable assumptions,[13] L may be computed from a standard EMD simulation by a generalized Green–Kubo relation[12]

$$L = \frac{V}{3}\int_0^\infty dt' \langle \mathbf{J}(t') \cdot \mathbf{J}(0) \rangle, \tag{4}$$

[a)]Electronic mail: ed@nd.edu

where V is the system volume. Equation (4) is obtained through invocation of linear response theory, so it is valid only in the limit of small chemical potential gradients. By writing the flux $\mathbf{J}$ in terms of the molecular velocity $\mathbf{v}_i$, defining the chemical potential in terms of the fugacity, and substituting Eq. (4) into Eq. (3), we obtain

$$D_t=\frac{1}{3N}\left\langle \int_0^\infty dt' \left\langle \sum_{i=1}^{N} \mathbf{v}_i(t')\cdot\sum_{j=1}^{N} \mathbf{v}_j(0) \right\rangle \right\rangle \left(\frac{\partial \ln f}{\partial \ln c}\right)_T, \tag{5}$$

where f is the fugacity and N is the number of molecules in the system.

This method has the advantage that it has a firm statistical mechanical basis, is straightforward to implement, and because it is an equilibrium method, allows the user to compute a host of other equilibrium properties from a single simulation. The drawback is that the integral in Eqs. (4) or (5) can be quite difficult to compute. EMD has been successfully used by several authors for computing nonequilibrium transport coefficients of confined fluids.[9,14–16]

In the expression for D_t [Eq. (5)], the correlation function inside the pointed brackets may be split into separate autocorrelation and cross-correlation parts, thereby resulting in

$$D_t=\left\langle \frac{1}{3N}\sum_{i=1}^{N}\int_0^\infty dt' \langle \mathbf{v}_i(t')\cdot\mathbf{v}_i(0)\rangle + \frac{1}{3N}\sum_{i=1}^{N}\sum_{j\neq i}^{N}\int_0^\infty dt' \langle \mathbf{v}_i(t')\cdot\mathbf{v}_j(0)\rangle \right\rangle \left(\frac{\partial \ln f}{\partial \ln c}\right)_T. \tag{6}$$

Note that the autocorrelation term in the above equation represents the *self-diffusivity* D_s. In the dilute limit where c tends to zero, the cross-correlation term in Eq. (6) tends to zero and $(\partial \ln f/\partial \ln c)_T$ approaches unity. Hence, in the dilute limit, the transport diffusivity tends to approach the self-diffusivity. The two diffusivities should not be confused with each other at finite concentrations as one is an individual property (D_s), while the other is a collective property (D_t).

B. Transient molecular dynamics

A second method proposed for computing nonequilibrium transport coefficients involves the use of a transient molecular dynamics technique.[12] In this method, an actual concentration gradient is set up within a simulation cell. The system is then allowed to relax using MD, and the rate of relaxation is monitored and fit to the appropriate continuum solution of the diffusion equation. In this way, D_t can be extracted directly from a single simulation. The method has a good physical basis and, in principle, is more computationally efficient than EMD simulations. It suffers from a number of practical issues, however, including difficulties in setting up an initial concentration profile and uncertainty about whether or not the simulation is occurring in the linear response regime. Transient MD techniques have been shown to be more efficient than EMD and NEMD methods in computing other collective properties such as shear viscosity.[17]

C. External field nonequilibrium molecular dynamics

A third technique for obtaining L is to drive the system using an external field. In this approach, an external field $\mathcal{F}$ that mimics the influence of a chemical potential gradient is introduced into the Hamiltonian. The system responds to this external perturbation by developing a homogeneous flux. Once the steady-state value of this flux has been measured, the coefficient L is then computed using Eq. (2) by replacing the "$-\nabla\mu$" term in the equation by the external force term "$\mathcal{F}$." The method is similar in spirit to other nonequilibrium methods used to compute collective transport properties such as viscosity.[18] Complete details of the method as applied to transport in microporous hosts may be found elsewhere.[12] The advantages of this technique are that it is easy to implement, computationally efficient, and a range of gradients may be used. The latter feature enables one to examine both linear and nonlinear responses. This method has not been widely used, perhaps because the equivalence of such a homogeneous external forcing function that drives diffusion and an actual chemical potential gradient has not been formally demonstrated. One of the objectives of the present study is to investigate whether the use of an external field in place of an actual chemical potential gradient is justified.

D. Boundary-driven nonequilibrium molecular dynamics

The fourth technique for obtaining nonequilibrium transport coefficients is through use of boundary-driven methods.[19–21] As applied to the study of transport in porous materials, this method involves the construction of high and low concentration reservoirs on opposite sides of a "transport zone." Molecules flow between the reservoirs and, as long as the population of the reservoirs is replenished, a steady-state flux develops. By computing the steady-state flux and through knowledge of the chemical potential (or concentration) gradient between the reservoirs, the transport coefficient may be evaluated directly as is consistent with the basic assumption of irreversible thermodynamics [see Eq. (2)]. This method has been enthusiastically adopted by many researchers, and is currently the most commonly used of the four techniques listed above for computing nonequilibrium transport coefficients. It has been used to study diffusion in zeolites,[22] membranes,[21,23–27] polymers,[28] microporous carbon and slit pores[29–33] and fluid systems.[34,35] The boundary-driven approach owes its popularity to the fact that it is a conceptually attractive method. Concentration or chemical potential gradients are established that mimic a real system, and the flux develops as a natural consequence.

There are several limitations of this method though. First, the number of molecules that must be simulated is larger than in any of the other approaches, due to the fact that reservoirs of molecules are required to maintain a density gradient. Second, the overhead associated with keeping the reservoirs properly populated (usually performed through a grand canonical Monte Carlo or GCMC procedure) is a significant fraction of the total simulation cost. This can be especially troublesome for complex molecules or dense systems, where the probability of achieving an accepted inser-

tion of a molecule using a grand canonical procedure can be very low. Recent work has been directed at overcoming this problem,[35] although many difficulties still remain. Third, the near-equilibrium approximation of irreversible thermodynamics that stipulates a linear relationship between the diffusive flux and the chemical potential gradient is often disrupted by real or artificial momentum transfers (as will be shown later in this paper). In general, momentum transfer can be included in the Onsager formalism of irreversible thermodynamics but this would require the determination of additional transport coefficients which are difficult to estimate. The best strategy to obtain an accurate value of L is therefore to identify such momentum transfers and to remove them artificially in these simulations. Finally, there are choices to be made about how to handle the reservoirs and the way they are interfaced with the transport region of the simulation box. These choices impact the performance of the simulation and the results that are obtained.

The first such choice to be made is the ratio of Monte Carlo to molecular dynamics moves or, in other words, the equilibration rate. Ideally, one would like this MC:MD ratio to be large so that the reservoirs are maintained at a fixed chemical potential.[29] If the ratio becomes too large, however, the computational requirements become overwhelming. Different authors have used different MC:MD ratios, and these ratios are often varied depending on the system being studied. Generally speaking, the greater the rate of transport, the higher the ratio should be.[20] Cracknell and co-workers used MC:MD ratios ranging from 20:1 to 110:1.[29] Xu and coworkers varied their MC:MD ratio from 50:1 to 400:1, depending on the size of the confining pore.[31] Heffelfinger and van Swol have used a ratio of 100:1 in examining a fluid system.[20] Thompson and co-workers used a ratio of 3072:1 to study binary diffusion.[34]

The second choice that must be made when performing such a simulation is how to assign the velocities of the molecules that are inserted in the reservoirs. Generally, molecular velocities are chosen from a Maxwell–Boltzmann distribution consistent with the thermodynamic temperature of the system. Some authors also add a ''streaming velocity'' to inserted molecules[29,31] while others do not.[20,34] It has been argued that the addition of streaming velocities to newly inserted molecules is necessary to avoid discontinuities in velocities at the reservoir/transport region interface, and that failure to add these streaming velocities leads to severely underestimated fluxes.[31] The addition of the proper streaming velocity is nontrivial, however, since the streaming velocity (i.e., flux) is the object of the simulation and so is not known *a priori*.[29] Typically, an iterative procedure is used, although such a method is prone to numerical instabilities.[29]

In summary, boundary-driven methods are conceptually attractive and simple, but the approach can be more computationally intensive than other techniques. Furthermore, the fact that the results can depend on how the reservoirs are interfaced with the transport region means that one must be very careful in how a simulation is conducted.

Given the variety of simulation methods available for calculating nonequilibrium transport coefficients in confined media, the obvious question is: which method is best? Surprisingly, there has not been a study in which these methods have been critically compared against one another in terms of accuracy and performance. There have been some comparisons made between results obtained using boundary-driven and EMD methods,[20,29,31] but these comparisons were generally limited to the self-diffusivity to ensure that the boundary-driven simulation was working properly. The objective of the present study is to critically compare the accuracy and performance of three techniques for computing nonequilibrium transport coefficients in confined media. The three techniques examined are equilibrium molecular dynamics (EMD), external field nonequilibrium molecular dynamics (EF–NEMD), and boundary-driven molecular dynamics in the form of the commonly used dual control volume grand canonical molecular dynamics (DCV–GCMD) algorithm. We also intend to study in detail the role of MC:MD ratio and streaming velocity on the DCV–GCMD results. We do not believe that transient methods of the kind described above are as useful for these types of simulation, and so we will not examine the use of this approach.

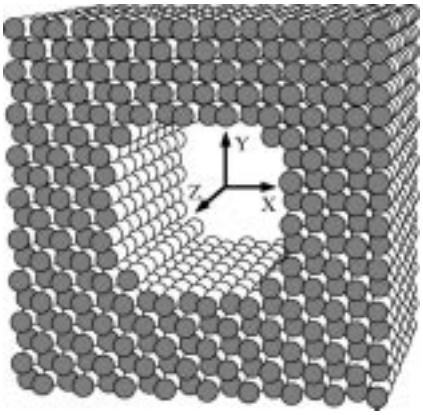

FIG. 1. Schematic showing the pore structure of Model 1. The shaded atoms comprise a unit cell.

II. MODEL AND SIMULATION DETAILS

Simulations were carried out in two different model pore systems. Model 1 consisted of a single pore cut through a face-center-cubic (fcc) lattice of oxygen atoms. The use of such a pore system enabled the diameter of the pore to be varied easily, so as to gauge the impact of pore diameter on the different simulation results. Nominally cylindrical pores of radius r_p along the z axis were created by removing oxygen atoms from the fcc lattice whose centers were less than r_p away from the pore axis. The Model 1 lattice is made up of several unit cells aligned along the z direction, where the width of the unit cell in the x and y directions fully encompasses the pore. It is important to keep the lattice width in the x and y directions larger than the diameter of the pore plus the cutoff radius of the potential (see below). The spacing between adjacent oxygen atoms, w, is fixed at 3.2 Å. Thus the length of the unit cell in the z direction is equal to 4.525 Å ($=w\sqrt{2}$), the true fcc unit cell length. The lattice is assumed to be rigid and defect free. Figure 1 shows a schematic of the structure of the pore and the oxygen lattice. Also shown in the same figure is a single unit cell as depicted by

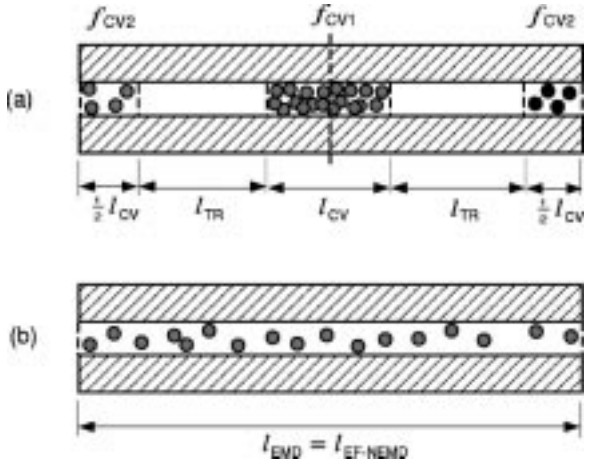

FIG. 2. Schematic diagram showing (a) the DCV–GCMD simulation cell, and (b) the EMD or EF–NEMD simulation cell.

the shaded oxygen atoms. Note that after removing the oxygen atoms from the lattice to form the pore, the resulting pore cross section does not remain perfectly circular but has some corrugations.

Pore Model 2 consisted of an actual zeolite pore ($AlPO_4$-5), which has a simple pore structure consisting of nonintersecting and approximately cylindrical pores of nominal diameter 7.3 Å running in the [001] direction. The unit cell of $AlPO_4$-5 has lattice parameters $a=13.726$ Å, $b=13.726$ Å, $c=8.484$ Å, $\alpha=90°$, $\beta=90°$ and $\gamma=120°$. Consistent with many past studies, the zeolite was modeled as a rigid lattice of oxygen atoms.[36] The $AlPO_4$-5 simulations serve as a check to ensure that the results obtained in the present work are general and applicable to real porous materials.

The diffusing guest species was a Lennard-Jones sphere with self-interaction parameters $\sigma=3.73$ Å and $\epsilon/k_B=147.95$ K[37] chosen to represent methane. Interactions between methane and the host oxygen atoms for both model systems were treated using parameters from Ref. 37, namely $\sigma=3.214$ Å and $\epsilon/k_B=133.3$ K. The potential cutoff radius was taken to be 10 Å. To reduce computational effort, a pretabulated potential map with a grid spacing of 0.2 Å was used.[38] Interactions between species in neighboring pores were neglected to save computational time. Although it is possible for molecules in neighboring pores of $AlPO_4$-5 to come slightly closer than the potential cutoff distance, these interactions are very small compared to those due to the pore walls and sorbates in the same pore, and so are not expected to have a significant impact on the transport properties.[39]

The simulation box for all the simulations consisted of an array of unit cells along the *z* direction. Periodic boundary conditions were applied in the *z* direction, while no periodic boundary conditions were required in the *x* and *y* direction as the sorbate molecules were confined within the pore. Figure 2(a) is a schematic of the simulation cell used for the DCV–GCMD simulations, while Fig. 2(b) shows the cell corresponding to the EMD and EF–NEMD simulations. The DCV–GCMD simulation cell consists of two transport regions, each sandwiched between two control volumes. The control volume in the middle of the simulation cell is referred to as CV1, while the two control volumes at the ends are referred to as CV2. CV1 is maintained at a high fugacity f_{CV1}, while the end control volumes CV2 are maintained at a lower fugacity f_{CV2}. The length of the control volumes is l_{CV} while the length of the transport region is l_{TR}.

A velocity Verlet algorithm with a time step of 5 fs was used to integrate the equations of motion. The equations of motion for the EF–NEMD simulations are the same as for the other two methods, except that an additional force in the *z* direction ($\mathcal{F}=-\nabla\mu$) is added to each molecule. To maintain a constant temperature, a Nosé–Hoover thermostat[40] with a time constant of 0.5 ps was used in all the simulations. For the EF–NEMD and DCV–GCMD simulations (where molecular fluxes develop) the temperature is defined by subtracting off the streaming velocity from the *z* component of the velocities. All simulations were performed at 300 K.

To compare the results for the different methods, the MS mobility coefficient was computed for each simulation method under the same nominal conditions. The mobility coefficient was computed using EMD through direct application of a Green–Kubo formula similar to Eq. (4),

$$L=V\int_0^\infty dt'\langle J_z(t')J_z(0)\rangle, \tag{7}$$

where now only the *z* component of the flux and mobility tensor is relevant. For the EF–NEMD simulations, the mobility coefficient was determined by first computing the steady-state flux that developed upon application of the external force $\mathcal{F}$ (assumed to drive molecules in the positive *z* direction), using the following equation:

$$J_z=\frac{N^+-N^-}{t_{\text{run}}A_{xy}}, \tag{8}$$

where t_{run} is the simulation run time over which the fluxes are recorded and A_{xy} is the cross-sectional area of the pore, approximated as πr_p^2. N^+ and N^- represent the net number of sorbate molecules that move through a flux plane within the pore in the positive and negative *z* directions, respectively. The MS mobility coefficient was then obtained from the measured flux as discussed in Sec. I. For the DCV–GCMD simulations, the steady-state flux that developed as a result of a chemical potential gradient $\nabla\mu=(\mu_{CV1}-\mu_{CV2})/l_{TR}$ was computed using Eq. (8), with the flux taken as the average of the fluxes recorded at planes located in the middle of the two transport regions. The MS mobility coefficient was then obtained from Eq. (2). Typically, simulation times on the order of 10–100 ns were required to obtain reliable flux values.

To make the comparison with the EMD simulations valid, it is crucial to ensure that the EF–NEMD and DCV–GCMD simulations are in the linear response regime. To check this for the DCV–GCMD simulations, simulations at three different chemical potential gradients were performed. The actual conditions are shown in Table I, where "*L*" designates low gradient simulations, "*M*" medium gradient simulations, and "*H*" high gradient simulations. The results described below show that, within the accuracy of the simulations, the computed transport coefficients are independent

TABLE I. Fugacities maintained in the two control volumes (f_{CV1} and f_{CV2}), the magnitude of the chemical potential difference ($\Delta\mu$) relative to k_BT, and the chemical potential gradient ($\nabla\mu$) produced for the different simulations.

Model system	Gradient level	f_{CV1} (bar)	f_{CV2} (bar)	$\Delta\mu/k_BT$	$\nabla\mu$ (J/mol/m)
Model 1	*L*	65.0	55.0	0.1671	2.3018×10^{11}
	M	70.0	50.0	0.3365	4.6361×10^{11}
	H	75.0	45.0	0.5108	7.0385×10^{11}
Model 2 (*LL*)	*L*	2.2	1.8	0.2007	2.9497×10^{11}
	M	2.4	1.6	0.4055	5.9601×10^{11}
	H	2.6	1.4	0.6190	9.0995×10^{11}
Model 2 (*HL*)	*L*	72.0	48.0	0.4055	5.9601×10^{11}
	M	76.0	44.0	0.5465	8.0339×10^{11}
	H	80.0	40.0	0.6931	1.0189×10^{12}

of the gradient, confirming that the system is in the linear response regime. The EF–NEMD simulations were performed using the same nominal chemical potential gradient as the DCV–GCMD simulations, and were also found to be in the linear response regime.

The $AlPO_4$-5 simulations were performed at two different sorbate loadings, where the low loading simulations were designated by the symbol ''*LL*'' while the high loading simulations were designated by the symbol ''*HL*.'' Model 1 simulations at each pore radius were however performed at a single loading (refer to Table I). The EMD and EF–NEMD simulations were performed at the same average sorbate loading as the DCV–GCMD simulations. In all cases, four different simulations were conducted, each starting from a different initial configuration. The results of these individual simulations were averaged to get the reported values. The lengths of the transport region in the DCV–GCMD simulations were fixed at $l_{TR}=18.10$ Å and $l_{TR}=16.97$ Å for Model 1 and Model 2, respectively, while the size of the control volumes was varied to accommodate a given loading. Other simulation details are provided in Table II.

TABLE II. EMD, EF–NEMD, and DCV–GCMD simulation details for Model 1 simulations at the five different pore radii (r_p), and Model 2 simulations at the two different sorbate loadings.

	r_p (Å)	l_{CV}[a] (Å)	l_E[b] (Å)	c_{avg}[c] (molec./UC)	t_D[d] (ns)	t_E[e] (ns)
Model 1	2.00	126.7	398.2	0.77	100(50)	100(50)
	4.56	54.3	144.8	2.07	50(25)	50(25)
	6.70	36.2	90.5	3.25	50(25)	50(25)
	9.35	27.2	63.4	5.11	25(12)	25(12)
	15.56	18.1	36.2	9.70	10(5)	10(5)
Model 2 (*LL*)	3.65	339.36	1153.8	0.53	250(100)	100(50)
Model 2 (*HL*)	3.65	67.87	169.7	3.56	250(100)	100(50)

[a]Length of control volumes in the DCV–GCMD simulations.
[b]Length of EMD and EF–NEMD simulation cell.
[c]Sorbate loading (equal in the EMD, EF–NEMD, and DCV–GCMD simulations).
[d]DCV–GCMD simulation run length. Equilibration times are in parentheses.
[e]EMD and EF–NEMD simulation run length. Equilibration times are in parentheses.

Two different types of DCV–GCMD simulations were conducted to test the importance of the use of a streaming velocity and the MC:MD ratio. The first set of simulations were standard DCV–GCMD simulations without the addition of a streaming velocity, and at three different MC:MD ratios. These simulations are denoted with the prefix ''DCVNS'' where NS stands for ''no streaming'' velocity. Simulations designated as DCVNS1 are associated with a very low grand canonical Monte Carlo overhead of 100 insertion/deletion attempts every 50 MD time steps. DCVNS2 simulations employed 500 MC insertion/deletion moves every 50 MD time steps, whereas DCV3NS simulations used 500 MC moves every 10 MD time steps. A second set of three DCV–GCMD simulations, denoted by the prefix ''DCVWS'' where WS stands for ''with streaming'' velocity, were performed at identical MC:MD ratios as the corresponding DCVNS simulations, but a streaming velocity consistent with the flux in the transport region was added to each *newly* inserted molecule. The streaming velocity was calculated as the average flux measured in the previous 1000 time steps divided by the average concentration in the control volume. Molecules were given a positive or negative streaming velocity depending on which side of the control volume center line they were added (see Fig. 2).

Finally, in an effort to better understand the results obtained from the different methods, a hybrid simulation technique was created that combines elements of the EF–NEMD and DCV–GCMD methods. This technique is designated with the prefix ''DEF.'' In the hybrid simulations, a simulation cell identical to that used in the DCV–GCMD simulations is used. Unlike the DCV–GCMD simulations, however, the two control volumes are maintained at *equal* chemical potentials through the use of a GCMC routine. The sorbate loading therefore remains uniform throughout the system, in contrast to the DCV–GCMD simulations. A force equal to the desired chemical potential gradient is added to the molecules within the transport region, and the resulting steady state flux was recorded and used to determine a transport coefficient via Eq. (2). In particular, we conducted one such type of simulation, whereby we used the *same* MC:MD ratio as in the DCVNS1 simulations, and *no* streaming velocity was added to newly inserted molecules in the control volumes (hence the simulation is designated as DEFNS1). The DEFNS1 simulations mimic the EF–NEMD simulations with the exception that control volumes are added to the ends of the transport regions. The DEFNS1 simulations also mimic the DCVNS1 simulations, except that an external force replaces an actual chemical potential gradient as the driving force for diffusion.

III. RESULTS AND DISCUSSION

A. Simulation results

Table III lists the computed values of the transport coefficient L as a function of pore size, gradient level, model type, and simulation method. The error bars on the results were estimated by computing the variance of four simulation runs, each starting from a different initial configuration. In

TABLE III. Computed transport coefficients from the EMD, EF–NEMD, DCV–GCMD, and the hybrid methods in the two model systems. The numbers in parentheses represent statistical uncertainties in the value of the transport coefficients.

	r_p (Å)	Gradient level	Transport coefficient L [$10^4\times$(mol/m/s)]								
			EMD	EF–NEMD	DEFNS1	DCVNS1	DCVNS2	DCVNS3	DCVWS1	DCVWS2	DCVWS3
	2.00	*L*		23.78(0.65)	10.17(0.78)	10.81(1.63)	11.08(1.43)	14.56(0.63)	11.63(0.34)	15.55(0.77)	21.51(2.41)
		M	22.25(1.55)	21.99(0.18)	9.59(0.17)	10.19(0.63)	12.46(0.54)	13.56(0.31)	10.64(0.97)	15.36(0.30)	22.13(1.71)
		H		21.15(0.22)	9.73(0.55)	10.55(0.37)	12.32(0.37)	13.65(0.45)	10.77(0.32)	16.19(0.73)	22.13(0.26)
	4.56	*L*		15.43(0.28)	8.85(0.28)	9.37(0.69)	9.02(0.24)	9.34(0.29)	12.40(0.11)	16.16(1.11)	15.63(1.19)
		M	16.08(1.17)	15.60(0.44)	8.67(0.43)	8.85(0.22)	8.96(0.06)	9.57(0.10)	12.12(0.04)	15.09(0.75)	16.08(0.25)
		H		15.72(0.13)	8.72(0.23)	9.03(0.20)	8.86(0.19)	9.71(0.19)	12.06(0.03)	14.20(0.06)	16.19(0.26)
	6.70	*L*		8.20(0.28)	5.31(0.14)	5.31(0.23)	5.98(0.55)	6.41(0.56)	7.83(0.18)	8.54(1.52)	8.86(0.40)
Model 1		*M*	9.64(1.08)	8.66(0.24)	5.52(0.18)	5.68(0.23)	5.89(0.32)	6.12(0.22)	7.32(0.20)	8.43(0.45)	9.23(0.53)
		H		8.88(0.15)	5.47(0.21)	5.79(0.08)	5.63(0.16)	5.93(0.30)	7.47(0.25)	8.46(0.09)	9.06(0.20)
	9.35	*L*		11.93(0.49)	6.07(0.12)	5.86(0.83)	6.49(1.01)	6.31(0.40)	9.01(0.76)	10.69(1.29)	13.22(1.83)
		M	13.16(0.83)	12.54(0.16)	6.25(0.17)	6.90(0.07)	6.15(0.31)	6.70(0.33)	9.65(0.36)	11.00(0.56)	12.50(0.47)
		H		12.74(0.20)	6.06(0.12)	6.21(0.13)	6.37(0.18)	6.63(0.13)	9.31(0.16)	10.69(0.37)	11.74(0.54)
	15.56	*L*		10.57(0.14)	4.61(0.24)	4.68(0.28)	4.95(0.22)	5.20(0.16)	7.23(0.33)	8.71(0.26)	9.72(0.27)
		M	10.94(0.83)	10.88(0.09)	4.43(0.03)	4.45(0.23)	4.71(0.12)	5.05(0.23)	7.03(0.25)	8.30(0.33)	9.29(0.09)
		H		10.92(0.08)	4.41(0.07)	4.56(0.08)	4.61(0.08)	4.87(0.10)	6.87(0.11)	8.25(0.11)	9.15(0.11)
	3.65	*L*		1.02(0.07)	0.78(0.09)	0.79(0.07)	0.88(0.07)	0.79(0.12)	0.96(0.13)	0.84(0.09)	0.97(0.01)
Model 2 (*LL*)		*M*	1.21(0.11)	1.11(0.04)	0.80(0.05)	0.80(0.01)	0.78(0.03)	0.82(0.03)	0.86(0.06)	092(0.07)	0.87(0.05)
		H		1.12(0.04)	0.77(0.04)	0.80(0.03)	0.77(0.03)	0.77(0.04)	0.82(0.02)	0.88(0.02)	0.88(0.02)
	3.65	*L*		1.61(0.09)	1.34(0.03)	1.45(0.08)	1.51(0.05)	1.68(0.07)	1.48(0.08)	1.70(0.12)	1.80(0.05)
Model 2 (*HL*)		*M*	1.87(0.10)	1.71(0.09)	1.34(0.04)	1.46(0.08)	1.62(0.02)	1.71(0.03)	1.49(0.02)	1.67(0.03)	1.80(0.03)
		H		1.77(0.06)	1.36(0.02)	1.44(0.01)	1.64(0.03)	1.71(0.04)	1.54(0.05)	1.65(0.02)	1.88(0.01)

the case of EMD simulations, the error bars were computed by taking the standard deviation of plateau values of the integral in Eq. (7) at an appropriately chosen simulation time. A time of 50 ps seemed reasonable as the integrals were observed to have reached near-steady values at that time. Measuring values of the integral at larger times resulted in large statistical errors, while shorter times led to systematic errors due to the neglect of long time tails.[40] The error bars on the EF–NEMD and DCV–GCMD results were computed from the variance of block averages of the fluxes obtained from the four runs.

There is generally good agreement between the transport coefficients computed using EMD and EF–NEMD simulations for all the pore radii and for both models. Note that the EF–NEMD results have smaller error bars as compared to the EMD method, suggesting that EF–NEMD is the more accurate of the two methods. The agreement between the DCV–GCMD results and the EMD or EF–NEMD results is on the other hand far from satisfactory. It is observed that the flux computed from the simulations with the low MC:MD ratio and no streaming velocity (DCVNS1) is lower than the flux from the EMD and EF–NEMD simulations by factors ranging roughly from 1.4 to 2.3. This is true for both Model 1 and Model 2, although the differences are smaller for Model 2. The DCVNS1 and DCVWS1 results in Table III show that keeping the MC:MD ratio constant but imposing a streaming velocity *increases* the computed transport coefficient. The magnitude of the increase ranges from less than 10% for the smallest pores to roughly 60% for the largest pores. This observation of confirms the assertion of Xu and co-workers that neglect of the streaming velocity leads to a lower computed flux.[31] The transport coefficients computed in the DCVWS1 simulations are still significantly smaller, however, than those obtained using the EMD or EF–NEMD methods.

To investigate the role that the ratio of stochastic to deterministic moves plays on the computed transport coefficient, the number of MC moves per 50 MD time steps was increased from 100 to 500 in the DCVWS2 simulations, and the frequency was increased in the DCVWS3 simulations such that 500 MC moves were performed every 10 MD time steps. In both cases, a streaming velocity was also added to inserted molecules. The results in Table III clearly show that, as the ''stochastic content'' of the simulation increases, the transport coefficient computed using the DCV–GCMD approaches that calculated using EMD and EF–NEMD. This can be more clearly observed in Fig. 3 where EMD, EF–NEMD, and DCV–GCMD results have been plotted along side each other. To show that the DCVWS-type simulation results asymptotically approach the EMD and EF–NEMD results as the MC:MD ratio is increased, and that L does not increase indefinitely with the MC:MD ratio, we plotted L obtained from DCV–GCMD simulations for the case of Model 1 with a pore radii of 6.7 Å against MC:MD ratio in Fig. 4. The plot also shows an additional simulation result at an abnormally high MC:MD ratio of 500 insertion/deletion attempts every MD time step. It can be clearly observed that L does reach a steady value at high MC:MD ratios, and that

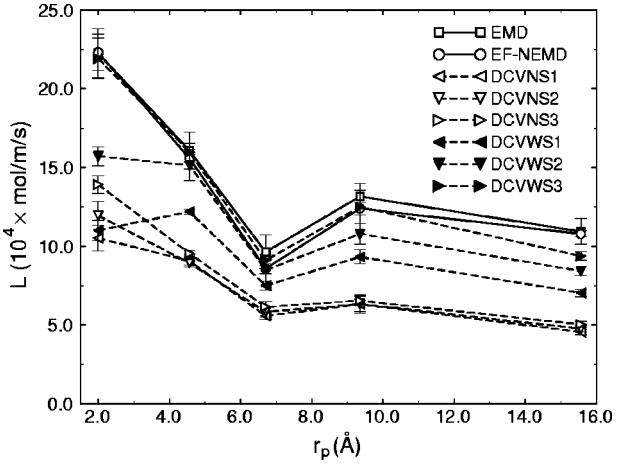

FIG. 3. Computed values of L for methane in Model 1 lattice from EMD, EF–NEMD, and the various DCV–GCMD simulations at different pore radii r_p. The solid and dashed lines are meant to guide the eye.

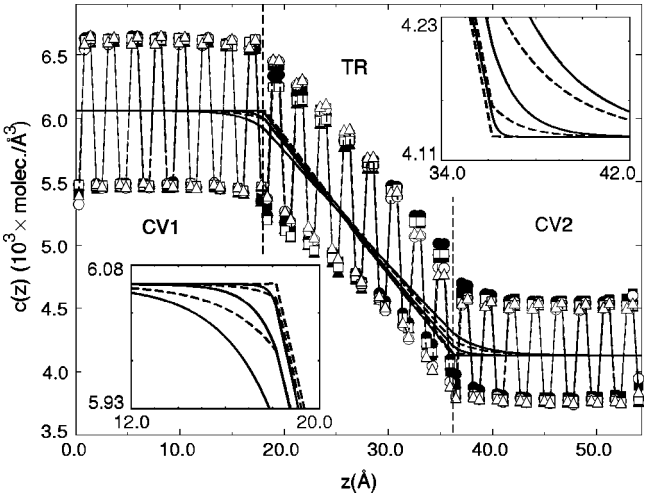

FIG. 5. Concentration profiles for the DCV–GCMD simulations. Solid symbols are representative of DCVNS-type simulations while open symbols are representative of DCVWS-type simulations. Circular symbols represent simulations at the lowest MC:MD ratio, square symbols represent simulations at the medium MC:MD ratio, while triangular symbols represent simulations at the highest MC:MD ratio. The insets show a close-up view of the two interfaces. The solid and dashed lines are the concentration profiles obtained from the RDC model for the DCVNS-type simulations and DCVWS-type simulations, respectively.

this value is commensurate with the EMD and EF–NEMD results. On the other hand, increasing the MC:MD ratio with *no* addition of a streaming velocity (as in DCVNS2 and DCVNS3 simulations) results only in little to moderate increases in the transport coefficient, and the transport coefficients at the highest MC:MD ratio are still significantly smaller than transport coefficients obtained via EMD and EF–NEMD methods (as seen clearly in Fig. 3). Hence, an increase in the MC:MD ratio profoundly impacts simulation results when the streaming velocity is implemented, but has only a small effect on simulation results when the streaming velocity is *not* implemented.

If one accepts that the EMD results are ''correct,'' then it is clear that the EF–NEMD method is able to obtain the correct transport coefficient, but that the value of the transport coefficient obtained from the DCV–GCMD simulations depends on the choice of whether a streaming velocity is added and what the MC:MD ratio is. To obtain the ''correct'' transport coefficient using DCV–GCMD, a large MC:MD ratio is required and a streaming velocity must also be used. This result is consistent with previous findings.[31,34] Unfortunately, the overhead associated with these operations is a significant fraction of the total simulation time. For example, the DCV–GCMD runs for the DCVWS1 simulations at $r_p = 6.7$ Å take roughly 3.5 h to complete on a SunULTRA30 workstation, whereas the DCVWS3 simulations with enhanced rates of insertions and deletions take about 7.5 h to complete. Increasing the frequency of insertions/deletions from 10 MD time steps to 1 MD time step (as is commonly done) increases the computational requirements even more, as these simulations now take roughly 50 h to complete. In contrast, equivalent EMD and EF–NEMD simulations took only about 1.5 h of CPU time to complete. This demonstrates that the EMD and EF–NEMD methods are significantly more efficient than the DCV–GCMD method for calculating nonequilibrium transport in microporous systems.

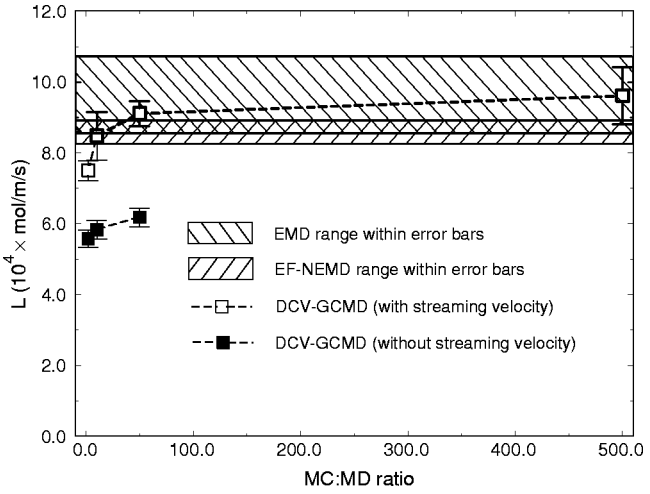

FIG. 4. Computed values of L for methane in Model 1 lattice with a pore radius of 6.7 Å from DCV–GCMD simulations at different MC:MD ratios. The MC:MD ratio was calculated as the number of insertion/deletion attempts per GCMC step divided by the number of MD time steps between two successive GCMC steps. The value of L obtained from EMD and EF–NEMD simulations are shown for reference. The dashed lines are meant to guide the eye.

To gain more insight into the DCV–GCMD results, we also obtained the concentration and flux profiles for the six different simulations, i.e., three DCVNS-type simulations plus the three DCVWS-type simulations. The profiles were obtained by dividing the axial length of the DCV–GCMD simulation cell into a number of bins of equal width. A bin width was chosen such that each unit cell of width 4.525 Å accommodated exactly eight bins. The concentration in each bin was computed by collecting the average number of molecules in the bins over the course of a simulation and then dividing it by the bin volume. The flux in each bin was measured by multiplying the average concentration by the average velocity, as measured in each bin. Figures 5 and 6 show the concentration and flux profiles obtained from the

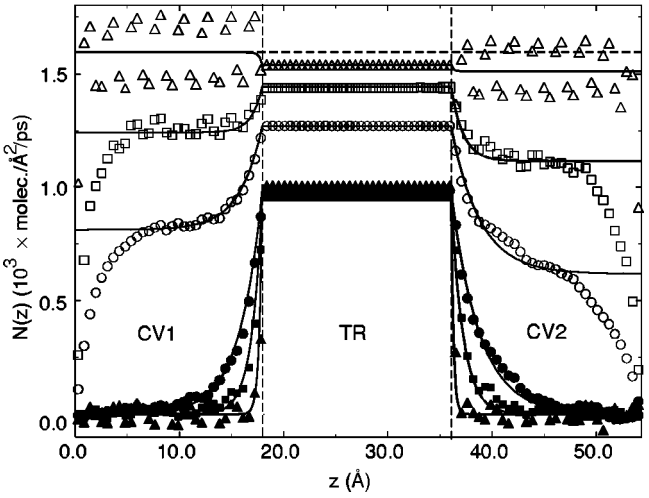

FIG. 6. Flux profiles for the DCV–GCMD simulations. Solid symbols are representative of DCVNS-type simulations while open symbols are representative of DCVWS-type simulations. Circular symbols represent simulations at the lowest MC:MD ratio, square symbols represent simulations at the medium MC:MD ratio, while triangular symbols represent simulations at the highest MC:MD ratio. The solid lines are the flux profiles obtained from the RDC model.

high (*H*) gradient DCV–GCMD simulations in a 6.7 Å radius pore of Model 1, respectively. Note that we only show the profiles on the right half of the DCV–GCMD simulation cell, knowing that the concentration and flux profiles on the left half of the simulation cell are, respectively, symmetric and antisymmetric to those on the right half. Concentration and flux profiles obtained from the rest of the DCV–GCMD simulations are not shown here, as they are very similar in nature to the ones shown for the present pore system.

It is noted that the concentration profiles fluctuate rapidly with large amplitudes due to corrugations in the pore potential thus making them almost indistinguishable from each other (refer to Fig. 5). In addition, these profiles are found to have poor resolution, especially at the interfacial regions between the transport region and the control volumes. In fact, the running averages of the profiles (not shown) also suffer from the above problems. We can observe from the existing plots that the concentrations in the control volume have been maintained fairly well in all the simulations, and that they exhibit an almost linear decay in the transport region. This linearity breaks down at the interfaces, suggesting significant momentum and mass transfers. In particular, we find that the concentrations at the control volume–transport region interfaces deviate from the concentrations within the bulk of the corresponding control volumes, i.e., the ''required'' concentrations. For example, the concentration at the CV1 interface is slightly *below* the required value, while the concentration at the CV2 interface is slightly *above* the required value. This is evidently because CV1 is not supplying molecules fast enough to the interface to account for the molecules being lost to the transport regions, and that CV2 is not depleting molecules fast enough to account for the molecules entering the lower concentration control volume. Another observation, though not clearly visible from Fig. 5, is that these interfacial concentrations approach their required values as the MC:MD ratio is increased. This is because the control volumes are now able to more thoroughly regenerate and deplete molecules at the interfaces as applicable.

The flux profiles plotted in Fig. 6 present a striking distinction between the six different simulations. The dotted horizontal line in the figure corresponds to the flux obtained in an ''idealized'' DCV–GCMD simulation with a transport coefficient equal to the average of transport coefficients obtained by EMD and EF–NEMD methods. This flux value of 1.595×10^{-3} molecules/Å^2/ps is denoted by the symbol N_0 for future reference. We note that the fluxes obtained in the transport regions for all DCV–GCMD simulations are lower than N_0, and that they approach N_0 when large MC:MD ratios as well as a streaming velocity are used. When a streaming velocity is not used, the three fluxes remain almost unchanged irrespective of the MC:MD ratio at about two-thirds of the N_0 value. We notice that the flux profiles for the DCVNS-type simulations decay to zero inside the control volumes due to the absence of any concentration gradients within the ''bulk'' of the control volume. This is not the case for the DCVWS-type simulations, where the fluxes remain nonzero in the control volumes. Clearly, this difference in the two profiles arises due to the presence of a streaming velocity in the DCVWS-type simulations, which gives rise to some form of convective flux developing in the control volumes. In the DCVNS-type simulations where a streaming velocity is not added, no such fluxes are observed. We also observe that the convective flux in the DCVWS-type simulations increases with the MC:MD ratio, evidently because a larger fraction of the molecules in the control volumes are the newly inserted molecules which possess a streaming velocity. In addition, we notice rather large fluctuations in the flux profiles within the control volumes for the simulations with large MC:MD ratios (i.e., the DCVNS3 and DCVWS3 simulations), apparently due to molecules not having enough time to develop a smooth flux profile. The fluxes abruptly tending to zero at the edges of the figure is an artificial boundary effect due to the requirement that the fluxes pass through a zero value at $z=0$ and $z=l_{\mathrm{CV}}+l_{\mathrm{TR}}$ to accommodate negative flux values in the left half of the simulation cell.

It is instructive to examine the results of the hybrid DEFNS1 simulations to better understand the source of the differences between the DCV–GCMD simulations and the other two techniques. Recall that in the DEFNS1 simulations, the flux is driven by the external field added to the Hamiltonian, as is done in EF–NEMD simulations, but the impact of having control volumes with molecular insertions and deletions is also incorporated, as is done in DCV–GCMD simulations. The results in Table III show that the transport coefficients obtained from DEFNS1 simulations are in good agreement with the DCVNS1 results, and that both results under predict L when compared to EMD and EF–NEMD. This result enables two important conclusions to be drawn. First, the assumption that $\mathcal{F}=-\nabla\mu$ in the EF–NEMD simulations is valid. That is, an external driving force in a system with homogeneous density produces the same type of flux response as does a system having an actual

TABLE IV. Parameters for the RDC model for the DCVNS-type and DCVWS-type simulations.

Simulation type	D_t (Å^2/ps)	k_1 (/ps)	k_3 (/ps)	v_1 (Å/ps)	v_2 (Å/ps)	v_3 (Å/ps)
DCVNS1	14.96	3.13	2.05	0.0	−0.067	0.0
DCVNS2	14.96	14.79	11.22	0.0	−0.104	0.0
DCVNS3	14.96	191.49	312.98	0.0	−0.111	0.0
DCVWS1	14.96	3.13	2.05	0.134	−0.035	0.150
DCVWS2	14.96	14.79	11.22	0.205	−0.025	0.270
DCVWS3	14.96	191.49	312.98	0.263	−0.013	0.366

chemical potential gradient, all other aspects of the systems being equal. This is a direct confirmation of the Maxwell–Stefan model, and proves the validity of the EF–NEMD method. Second, the fact that the DEFNS1 simulations *disagree* with the EF–NEMD results having the same external driving force indicates that the difference is due to the fact that the former method includes the effect of control volumes which the latter method excludes. Having just shown that the hybrid and DCV–GCMD methods are formally equivalent, the above statement *in turn* implies that the difference in the DCV–GCMD approach and the other methods *also* lies in the treatment of the control volumes.

In order to understand the role of control volumes in the DCV–GCMD simulations, a mass-transfer model has been developed. The model represents the DCV–GCMD simulations as a combination of reaction (R), diffusion (D), and convection (C) processes; henceforth the model is referred to as the RDC model. The model attempts to find an explanation as to why the transport coefficients L computed from the DCV–GCMD method increase and approach corresponding coefficients computed from EMD or EF–NEMD methods as the MC:MD ratio is increased when a streaming velocity is imposed, and why these transport coefficients do not show a similar increase when a streaming velocity is not imposed.

B. RDC model

The RDC model, in brief, assumes that the insertion and deletion mechanism in the two control volumes may be modeled as a first-order reversible reaction with parameters k_1 and k_3 representing the rates of insertions/deletions in CV1 and CV2, respectively. Diffusion is modeled using Fick's law with transport diffusivity D_t, while convection is represented by the convective velocities v_1, v_2, and v_3 in CV1, transport region and CV2, respectively. The above analysis ultimately leads to standard mass-transfer governing equations and boundary conditions in each of the three regions of the DCV–GCMD simulation cell, i.e., the two control volumes, and the transport region [Eqs. (A5)–(A13)]. Details on the derivation and implementation of the model are given in the Appendix.

The model was applied to the high (H) gradient DCV–GCMD simulations performed in the 6.7 Å pore of Model 1. These results are representative of the rest of the simulations conducted in this work, hence we chose to restrict our analysis to these conditions. The six parameters in the RDC model were obtained using the procedure outlined in the Appendix, and their values are given in Table IV. The solid lines in Figs. 5 and 6 show the concentration and flux profiles as predicted by the model. The agreement with the simulation results is excellent. Analysis of the model parameters given in Table IV indicates that the discrepancy between the DCV–GCMD simulations and the other methods is due to two types of resistances induced by the control volumes. The *first* resistance, denoted as the ''concentration resistance,'' arises from the fact that the control volumes are not able to replenish the concentration near the control volume–transport region interfaces fast enough to maintain the required concentrations at the two interfaces. The existence of such a resistance in the DCV–GCMD simulations is apparent from the concentration profiles in Fig. 5, shown in the insets. At small values of k_1 and k_3, which corresponds to a small MC:MD ratio, the interfacial concentration corresponding to CV1 becomes lower than the required value of $c_{-\infty}$. Likewise, the interfacial concentration corresponding to CV2 becomes higher than the required value of $c_{+\infty}$. This results in an actual concentration gradient that is *smaller* than the nominal value, which ultimately results in a lowering of the flux. An increase in the k value or the MC:MD ratio causes the interfacial concentrations to reach their required values, resulting in a lowering of this resistance. Addition of a streaming velocity to newly inserted molecules generates convection in the same direction as diffusion, which helps in further minimizing the concentration resistance. This convective flux helps in enhancing the interfacial concentrations by supplying molecules to the CV1 interfaces and transporting molecules away from the CV2 interface at higher rates compared to a purely diffusional mode of transport.

From the above arguments, we expect that the fluxes in both DCVNS-type and DCVWS-type simulations would asymptotically reach the N_0 value as the MC:MD ratio is increased. However, there is not much indication of an increase in the flux with the MC:MD ratio for the DCVNS-type simulations. In fact, in the case of DCVNS3 simulations the fluxes remain well below the N_0 value even though the interfacial concentrations at this high MC:MD ratio have been maintained very well. On the other hand, the DCVWS-type simulations correctly show this expected flux increase and its approach towards the N_0 value as the MC:MD ratio is increased. This immediately suggests the presence of some other type of resistance which becomes substantial for systems where a streaming velocity is not imposed on the newly inserted molecules.

The origin of this *second* form of resistance, referred to as the ''momentum resistance,'' may be explained by considering a molecule diffusing from CV1 towards the CV2 in a typical DCVNS-type simulation. This molecule, having attained a drift velocity in the transport region, given by $N(z)/c(z)$, is likely to get deleted in the end control volume and replaced by a molecule with a random velocity vector, i.e., with a zero drift velocity. Similarly, a molecule on the verge of leaving the middle control volume and entering the transport region would have attained some drift velocity within the control volume itself. However, this molecule also has some likelihood of getting deleted before it enters the transport region and replaced with a molecule with a zero drift velocity. This artificial means of maintaining concentra-

tion in the control volume through insertion and deletion of molecules leads to a net loss of z momentum in the control volumes, in addition to the z momentum loss that occurs due to collision of sorbate molecules with the zeolite walls in the control volumes. This effect results in a resistance wave which starts from CV2 and propagates upstream towards the CV1. This resistance wave manifests itself in the form of a ''backward convection,'' that is a convective flux in the opposite direction as shown by the large negative values of v_2 in the model for the DCVNS-type simulations. The momentum resistance should therefore *increase* with the MC:MD ratio as the chances for a molecule getting deleted and reinserted with a zero net velocity increase with the MC:MD ratio. We can easily observe this trend from the magnitude of the convective velocity, v_2, which increases with the insertion/deletion rate for the DCVNS-type simulations.

In the DCVWS-type simulations, on the other hand, the momentum loss is much less severe since a streaming velocity consistent with the prevailing flux in the transport region is added to the newly ''reinserted'' molecules. The momentum introduced by the streaming velocity is essentially used to counteract the interfacial momentum resistance. At this stage, most of the z momentum loss that occurs is as a result of sorbate molecules colliding with the zeolite walls. As expected, we observe that the magnitude of the convective term v_2 is much lower in the DCVWS-type simulations as compared to the DCVNS-type simulations. It is also noted that as the MC:MD ratio is increased, the magnitude of the backward convective velocity decreases. This implies that the momentum resistance interestingly decreases with the MC:MD ratio in the DCVWS-type simulations, as opposed to the DCVNS-type simulations where a reverse trend is observed. This decrease in the momentum resistance with the MC:MD ratio may be explained by noting that with an increase in the MC:MD ratio, the probability of ''old'' molecules (with decaying streaming velocities) getting deleted and replaced by ''new'' molecules (with renewed streaming velocities) increases tremendously. In other words, the old molecules are provided with less time to lose their streaming velocity through collisions with the zeolite lattice. Furthermore, a smaller fraction of molecules in the control volumes consist of these old molecules.

To recap the above analysis, the concentration and momentum resistances work in an antagonistic fashion with respect to the MC:MD ratio in the simulations where no streaming velocity is added to newly inserted molecules. That is, as the MC:MD ratio is increased, the concentration resistance decreases while the momentum resistance increases, and vice versa. This helps to explain why some of the fluxes in the DCVNS-type simulations exhibit nonmonotonic dependence with the MC:MD ratio, and always remain lower than the corresponding N_0 values as the MC:MD ratio is increased. On the other hand, when a streaming velocity is imposed to the newly inserted molecules, the two resistances work together with respect to the MC:MD ratio. That is, both the resistances decrease with an increase in the MC:MD ratio, and vice versa. Consequently, the fluxes under the condition that a streaming velocity is imposed increase monotonically with the MC:MD ratio and approach the corresponding N_0 value asymptotically. In the limit when the number of insertion/deletion attempts per GCMC step is very large and that the GCMC routine is called every time step, the flux would ideally reach the limit of N_0. At this stage, the diffusive flux would be zero everywhere inside the control volume as the concentration resistance would also have been entirely eliminated due to the large MC:MD ratios used. Also, all the molecules in the control volume would be replaced every time step and thus the convective flux in the control volumes would be identical to the purely diffusive flux in the transport region. As a result, the flux profile would remain absolutely flat, spanning both the control volumes and the transport region. We notice that the DCVWS3 simulations are quite close to this stage (refer to Fig. 6). The simulations at this stage present no net loss of z momentum due to insertion and deletion of molecules in the control volumes, and hence start resembling the EF–NEMD simulations where no loss of momentum occurs due to momentum propagation across periodic boundary conditions.

Last, it is interesting to note that while the transport coefficients from the DCVNS1 simulations for the $AlPO_4$-5 pore are lower than the transport coefficients obtained from the EMD and EF–NEMD simulations, the differences are not as great as they are for the model pore system. A clue to the origin of this difference can be obtained by noting in Table III that the transport coefficient of methane in $AlPO_4$-5 pore is an order of magnitude lower than the transport coefficient in the model pore. The reason is that the $AlPO_4$-5 pore is more corrugated than the model pore, which gives rise to higher energy barriers for diffusion. Diffusion in $AlPO_4$-5 therefore takes place via infrequent activated ''jumps,'' while diffusion in the model pore is a more continuous process. This suggests that the concentration resistance in systems with large energy barriers for diffusion is small as compared to that in ''smoother'' pores, such as the model system. This is because the factor $\sqrt{k/D_t}$, which determines how fast molecules are replenished at the interfaces, is very large when D_t is small. Additionally, the momentum resistance is expected to be small when diffusional barriers are high, since diffusion takes place by a series of infrequent jumps. In between ''hops'' these molecules have little or no residual momentum, so their deletion does not impact the overall flux as much as it does for systems with low energy barriers.

The above reasoning has interesting implications when applied to systems where the microporous material introduces large energy barriers for diffusion of certain sorbates, as is the case with many sorbate–zeolite systems. These barriers could be due to constrictions in the pores or the presence of cations. For such systems, the contribution of both the concentration and the momentum resistance is expected to be small in the DCV–GCMD simulations. We therefore expect that the transport coefficients obtained from the baseline DCV–GCMD method, i.e., without streaming velocity and having low MC:MD ratios, will closely resemble those computed using the EMD or EF–NEMD method in sorbate-zeolite systems where the energy barriers are much larger than the ones in the methane–$AlPO_4$-5 system. This still does not change the fact, however, that the DCV–GCMD

method is *still* an inefficient method for obtaining transport coefficients.

IV. SUMMARY AND CONCLUSION

Three different molecular dynamics methods have been compared for the calculation of nonequilibrium transport coefficients in microporous materials. Two different pore systems were examined: an idealized pore of varying pore diameter formed from an fcc lattice of oxygen atoms, and an actual $AlPO_4$-5 zeolite pore. For all cases, the transport coefficients calculated from EMD and EF–NEMD agreed with each other. The transport coefficient computed in a DCV–GCMD simulation varied, depending on whether or not a streaming velocity was added to newly inserted molecules and what the stochastic:deterministic move ratio was. Transport coefficients calculated using the DCV–GCMD method agreed with the results from the other two techniques only in the limit of very high stochastic:deterministic move ratios and when streaming velocities were added to molecules inserted in the control volumes.

To explain the source of differences in the methods, results from a hybrid simulation technique that employs an external field to drive diffusion between two control volumes maintained at equal chemical potential were first compared with DCV–GCMD and EF–NEMD simulations under the same nominal conditions. The results obtained validated the EF–NEMD method, as well as the Maxwell–Stefan model commonly invoked to describe diffusion in microporous systems. The results also showed that the control volumes used in the DCV–GCMD simulations introduce some form of mass transfer resistance to transport. Next, we developed a simple mass-transfer model to understand in more detail the origin of this resistance. It was found that two types of mass transfer resistances exist in the DCV–GCMD method. The first form of resistance arises from the inability of the control volumes to maintain their interfacial concentration, while the second arises due to momentum losses caused by the insertion and deletion of molecules. It was shown that with the imposition of a streaming velocity to newly inserted molecules in the control volumes and the use of large stochastic:deterministic ratios, both forms of resistances can be eliminated. The model is able to correctly predict the concentration and flux profiles in the DCV–GCMD simulations. The model also predicts that the inaccuracies caused by neglect of a streaming velocity for inserted molecules along with a small MC:MD ratio in the DCV–GCMD simulations are reduced for systems with high activation barriers for diffusion.

It is reasonable to consider whether the fluxes in the EMD and EF–NEMD simulations are actually artificially *high* due to propagation of momentum across periodic boundaries. For simulating transport along a macroscopic pore, the use of periodic boundary conditions would seem to be justified, as this is a more physically realistic model than one in which there are stagnant ''control volume'' fluid elements spaced along the pore. On the other hand, the use of stagnant control volumes, where no streaming velocity is imposed to newly inserted molecules, would be appropriate for examining transport across well-mixed interfaces or where a stationary bulk fluid is in contact with a confined phase. In such systems, interfacial mass and momentum transfer effects as observed in the DCV–GCMD simulations become very important. This is especially true in microscale or mesoscale devices when the transport medium is short and the interfacial resistance may be as important as the resistance in the medium. For these cases, either a full DCV–GCMD simulation or a hybrid simulation (such as the DCNEF1 method) that utilizes an external force to drive diffusion and two reservoirs at the same nominal chemical potential are appropriate methods.

Finally, the computational performance of the three simulations was compared and it was determined that the DCV–GCMD method is much less efficient than either the EMD or EF–NEMD technique. For the systems examined here, the DCV–GCMD simulations took roughly 5 times more CPU time than the other methods to get similar results. This is due mainly to the overhead associated with maintaining control volumes at a given chemical potential. We conclude that EMD or EF–NEMD are the best methods to use when examining diffusion along a pore, and that boundary-driven techniques such as DCV–GCMD are better suited for examining interfacial transport, where the use of control volumes has a necessary physical basis.

ACKNOWLEDGMENTS

Acknowledgment is made to the donors of The Petroleum Research Fund, administered by the ACS, for partial support of this research. Computational resources were provided by a grant from the Army Research Office (No. DAAG55-981-0091). The Center of Applied Mathematics, University of Notre Dame, provided financial assistance and a graduate fellowship (G. A.). One of the authors (E. J. M.) acknowledges the National Science Foundation CAREER program (No. CTS-9701470) for their support. Another author (H.C.C.) acknowledges support from the Bayer chair fund. The authors also thank Marcus Martin and Aidan Thompson of Sandia National Laboratory for helpful discussions.

APPENDIX

In the RDC model, the GCMC routine can be modeled as a ''differential controller'' or a first-order reversible reaction that maintains the concentration of molecules at the ''set-point'' value, c_{avg}

$$\frac{dc}{dt} = -k(c - c_{\mathrm{avg}}), \tag{A1}$$

where c is the instantaneous concentration, k is a first-order rate constant dependent on the rate of insertions and deletions. Assuming that the concentration gradients are small, the diffusion of molecules may be modeled using Fick's law

$$J_z = -D_t(c)\frac{dc}{dz}, \tag{A2}$$

where J_z is the diffusive flux along the axis of the pore (i.e., the z direction) while $D_t(c)$ is the transport diffusivity of the molecules in the microporous material. We also include the

possibility of convection occurring within the pore. The convective flux can be expressed as $v_z c$, where v_z is the macroscopic convective velocity in the z direction. The total flux within the control volume in the z direction, N_z, is then given as the sum of diffusive and convective fluxes

$$N_z = J_z + v_z c = -D_t(c)\frac{dc}{dz} + v_z c. \tag{A3}$$

Combining Eqs. (A1) and (A3) under the assumptions of steady state, we obtain the following second-order differential equation which governs mass transport in the control volumes

$$D_t(c)\frac{d^2c}{dz^2} - v_z\frac{dc}{dz} - k(c - c_{\text{avg}}) = 0. \tag{A4}$$

The differential equation governing mass transport in the transport regions remains the same as in the control volumes with the exception that the reaction term vanishes since insertion and deletion of molecules is restricted to the control volumes only.

In the model we only consider the right half of the symmetric DCV–GCMD simulation cell shown in Fig. 2(a) for convenience. The domain of analysis can thus be divided into three distinct regions: the high concentration control volume [the right half of CV1 in Fig. 2(a)], the transport region, and the low concentration control volume [the portion of CV2 on the rightmost end in Fig. 2(a)]. These three regions, starting from CV1, are, respectively, denoted by the symbols "1," "2," and "3." To simplify our analysis, we consider that the regions 1 and 3 extend to $-\infty$ and $+\infty$, respectively. We assume that the concentrations at $z=-\infty$ and $z=+\infty$ are $c_{-\infty}$ and $c_{+\infty}$, respectively. These concentrations are also the set-point concentrations in regions 1 and 3. At the interface between regions 1 and 2 where $z=z_{-0}$, and at the interface between regions 2 and 3 where $z=z_{+0}$, we impose continuity of the concentration and total flux profiles. Therefore, the resulting governing equations in the three regions along with the boundary conditions are given by

$$D_t(c_1)\frac{d^2c_1}{dz^2} - v_1\frac{dc_1}{dz} - k_1c_1 = -k_1c_{-\infty}, \tag{A5}$$

$$D_t(c_2)\frac{d^2c_2}{dz^2} - v_2\frac{dc_2}{dz} = 0, \tag{A6}$$

$$D_t(c_3)\frac{d^2c_3}{dz^2} - v_3\frac{dc_3}{dz} - k_3c_3 = -k_3c_{+\infty}, \tag{A7}$$

$$c_1(z\to-\infty) = c_{-\infty}, \tag{A8}$$

$$c_1(z=z_{-0}) = c_2(z=z_{-0}), \tag{A9}$$

$$N_1(z=z_{-0}) = N_2(z=z_{-0}), \tag{A10}$$

$$c_2(z=z_{+0}) = c_3(z=z_{+0}), \tag{A11}$$

$$N_2(z=z_{+0}) = N_3(z=z_{+0}), \tag{A12}$$

$$c_3(z\to+\infty) = c_{+\infty}, \tag{A13}$$

where the six unknown parameters are D_t, v_1, v_2, v_3, k_1, and k_3. The above set of second-order differential equations along with their boundary conditions can be solved using a finite difference procedure once the six unknown parameters are known so as to obtain both the concentration and the flux profiles along the pore axis.

The transport diffusivity, D_t, was obtained as a function of c from the transport coefficient L using Eq. (3). Since the variation in the diffusivity across the transport region was found to be fairly small ($\sim$ a factor of 1.2 for the "H" DCV–GCMD simulations in the 6.7 Å pore of Model 1), we believe it is reasonable to assume a constant diffusivity for convenience. The value of D_t chosen for the model was taken as the mean of D_t values obtained from the EMD and EF–NEMD simulations. The convective velocities in the control volumes, v_1 and v_3, were obtained directly from the flux profiles shown in Fig. 6. For the DCVNS-type simulations, the convective flux tends to zero inside the control volumes, implying that the convective velocities v_1 and v_3 are equal to zero. This is not true for the DCVWS-type simulations, however, where the fluxes in the control volumes asymptotically approach nonzero values. The values of v_1 and v_3 for these simulations are therefore nonzero, and can be estimated by dividing the asymptotic flux value by the concentration. The parameters k_1 and k_3 for the DCVNS-type simulations cannot be determined in a rigorous manner. Therefore they were treated as adjustable parameters, and were obtained as follows.

With the prior knowledge that $v_1=v_3=0$ for the DCVNS-type simulations, it can easily be shown that the flux decays exponentially in the two-control volumes according to

$$N(z) = \begin{cases} N_{\text{tr}}\exp\left(\sqrt{\dfrac{k_1}{D_t}}(z-z_{-0})\right) & \text{if } z\leqslant z_{-0}, \\ N_{\text{tr}}\exp\left(\sqrt{\dfrac{k_3}{D_t}}(z_{+0}-z)\right) & \text{if } z\geqslant z_{+0}, \end{cases} \tag{A14}$$

where N_{tr} is the constant flux in the transport region. The flux profiles in the left and right control volumes were then fitted, respectively, to the two solutions given in Eq. (A14) so as to obtain the parameters k_1 and k_3. We shall assume here that k values obtained here for the DCVNS-type simulations remain unaltered with the addition of a streaming velocity for the corresponding DCVWS-type simulations.

The remaining parameter v_2 was then obtained by solving the full set of governing equations [Eqs. (A5)–(A13)] using the finite difference method, and then matching the flux profiles predicted by the model and those obtained from the simulations by adjusting the value of the unknown parameter.

[1] R. Haberlandt and J. Kärger, Chem. Eng. J. **74**, 15 (1999).
[2] D. M. Ruthven and J. Kärger, *Diffusion in Zeolites and Other Microporous Solids* (Wiley, New York, 1992).
[3] J. G. Tsikoyiannis and J. Wei, Chem. Eng. Sci. **46**, 233 (1991).
[4] J. Xiao and J. Wei, Chem. Eng. Sci. **47**, 1123 (1992).
[5] F. J. Keil, R. Krishna, and M-O. Coppens, Rev. Chem. Eng. **16**, 71 (2000).
[6] S. M. Auerbach, Int. Rev. Phys. Chem. **19**, 155 (2000).
[7] A. T. Bell, E. J. Maginn, and D. N. Theodorou, in *Handbook of Heterogeneous Catalysis*, edited by G. Ertl, H. Knözinger, and J. Weitkamp

(VCH, Weinheim, Germany, 1997), Vol. 3, pp. 1165–1188.
[8] S. R. De Groot and P. Mazur, *Nonequilibrium Thermodynamics* (North-Holland, Amsterdam, 1962).
[9] M. J. Sanborn and R. Q. Snurr, Sep. Purif. Technol. **20**, 1 (2000).
[10] F. Kapteijn, W. J. W. Bakker, G. Zheng, J. Poppe, and J. A. Moulijn, Chem. Eng. J. **57**, 145 (1995).
[11] R. Krishna, Chem. Phys. Lett. **326**, 477 (2000).
[12] E. J. Maginn, A. T. Bell, and D. N. Theodorou, J. Phys. Chem. B **97**, 4173 (1993).
[13] D. N. Theodorou, R. Q. Snurr, and A. T. Bell, in *Comprehensive Supramolecular Chemistry*, edited by G. Alberti and T. Bein (Pergamon, Oxford, 1996), Vol. 7, p. 507.
[14] D. S. Sholl, Ind. Eng. Chem. Res. **39**, 3737 (2000).
[15] S. Suzuki, H. Takaba, T. Yamaguchi, and S. Nakao, J. Phys. Chem. B **104**, 1971 (2000).
[16] J. P. Hoogenboom, H. L. Tepper, N. F. A. van der Vegt, and W. J. Briels, J. Chem. Phys. **113**, 6875 (2000).
[17] G. Arya, E. J. Maginn, and H.-C. Chang, J. Chem. Phys. **113**, 2079 (2000).
[18] D. J. Evans and G. P. Morriss, *Statistical Mechanics of Nonequilibrium Liquids* (Academic, New York, 1990).
[19] M. Lupkowski and F. van Swol, J. Chem. Phys. **95**, 1995 (1991).
[20] G. S. Heffelfinger and F. van Swol, J. Chem. Phys. **100**, 7548 (1994).
[21] J. M. D. MacElroy, J. Chem. Phys. **101**, 5274 (1994).
[22] J. R. Hill, A. R. Minihan, E. Wimmer, and C. J. Adams, Phys. Chem. Chem. Phys. **2**, 4255 (2000).
[23] J. M. D. MacElroy and M. J. Boyle, Chem. Eng. J. **74**, 85 (1999).
[24] P. I. Pohl and G. S. Heffelfinger, J. Membr. Sci. **155**, 1 (1999).
[25] S. Furukawa and T. Nitta, J. Membr. Sci. **178**, 107 (2000).
[26] J. M. D. MacElroy, Kor. J. Chem. Eng. **17**, 129 (2000).
[27] S. Murad and J. Lin, Chem. Eng. J. **74**, 99 (1999).
[28] D. M. Ford and G. S. Heffelfinger, Mol. Phys. **94**, 673 (1998).
[29] R. F. Cracknell, D. Nicholson, and N. Quirke, Phys. Rev. Lett. **74**, 2463 (1995).
[30] D. Nicholson, Carbon **36**, 1511 (1998).
[31] L. Xu, T. T. Tsotsis, and M. Sahimi, J. Chem. Phys. **111**, 3252 (1999).
[32] K. P. Travis and K. E. Gubbins, Mol. Simul. **25**, 209 (2000).
[33] L. Xu, M. G. Sedigh, T. T. Tsotsis, and M. Sahimi, J. Chem. Phys. **112**, 910 (2000).
[34] A. P. Thompson, D. M. Ford, and G. S. Heffelfinger, J. Chem. Phys. **109**, 6406 (1998).
[35] A. P. Thompson and G. S. Heffelfinger, J. Chem. Phys. **110**, 10693 (1999).
[36] A. V. Kiselev, A. A. Lopatkin, and A. A. Shulga, Zeolites **5**, 261 (1985).
[37] S. J. Goodbody, K. Watanabe, D. MacGowan, J. P. R. B. Walton, and N. Quirke, J. Chem. Soc., Faraday Trans. **87**, 1951 (1991).
[38] M. D. Macedonia and E. J. Maginn, AIChE J. **46**, 2504 (2000).
[39] G. Arya, E. J. Maginn, and H.-C. Chang, J. Phys. Chem. B **105**, 2725 (2001).
[40] M. P. Allen and D. J. Tildesley, *Computer Simulation of Liquids* (Clarendon, Oxford, 1987).